

Efficient Simulation of Coupled Circuit-Field Problems: Generalized Falk Method

Loc Vu-Quoc, Yuhu Zhai, and Khai D. T. Ngo, *Senior Member, IEEE*

Abstract—In this paper, we present an efficient method to solve the coupled circuit-field problem, by first transforming the partial differential equations (PDEs) governing the field problem into a simple one-dimensional (1-D) equivalent circuit system, which is then combined with the circuit part of the overall coupled problem. This transformation relies on the generalized Falk algorithm, which transforms the coordinates in any complex system of linear first-order ordinary differential equations (ODEs) or second-order undamped ODEs, resulting from the discretization of field PDEs, into guaranteed stable-and-passive 1-D equivalent circuit system. The generalized Falk algorithm, having a faster transformation time compared with the traditional Lanczos-type methods, transforms a general finite-element system represented by possibly a system of full matrices—capacitance and conductance matrices in heat problems, or mass and stiffness matrices in structural dynamics and electromagnetics—into an identity capacitance (mass) matrix and a tridiagonal conductance (stiffness) matrix. We also discuss issues related to the stability and the loss of orthogonality of the proposed algorithm. In circuit simulation, the generalized Falk algorithm does not produce unstable positive poles, and is thus more stable than the widely used Lanczos-type methods. The stability and passivity of the resulting 1-D equivalent circuit network are guaranteed since all transformed matrices remain positive definite. The resulting 1-D equivalent circuit system contains only resistors, capacitors, inductors, and current sources. The generalized Falk algorithm offers an extremely simple and convenient way to incorporate field problems into circuit simulators to efficiently solve coupled circuit-field problems. Numerical examples show a significant reduction of simulation time compared to the solution without using the proposed transformation.

Index Terms—<<AUTHOR, PLEASE SUPPLY YOUR OWN KEYWORDS OR SEND A BLANK E-MAIL TO KEYWORDS@IEEE.ORG TO RECEIVE A LIST OF SUGGESTED KEYWORDS>>.

I. INTRODUCTION

MANY applications in engineering require the solution of coupled circuit-field problems. With the recent advances in high-temperature semiconductor technology, there is growing need for power converters in high-temperature,

high-power-density applications. Due to the increasing current density and higher power requirements of advanced power semiconductor devices such as insulated gate bipolar transistor (IGBT) and metal oxide semiconductor field-effect transistor (MOSFET), the devices dissipate a considerable amount of heat. Regardless of the electrical quality of power semiconductor devices, devices will fail if heat cannot be removed effectively. In addition, the electrical performance of the system can be limited by device heating and thermal coupling between devices. Therefore, the coupling between circuit networks and the thermal field problem to examine potential self-heating problems in power semiconductor devices requires an accurate electrothermal simulation of complete power electronic systems [1], [2]. The dense three-dimensional packaging used in compact electronic systems often produces magnetic interactions that interfere with system performance, and thus requires accurate simulation of this coupled circuit-field problem. Most nonlinear semiconductor device models are implemented in circuit simulators that are widely used by engineers. Many of these simulators have highly efficient solvers. Thus, it is advantageous if coupled circuit-field problems using circuit simulators. To this end, methods to develop circuit networks equivalent to discretized field equations have been proposed [2], [3]. Even for certain field problems alone, such as structural dynamics, it has been demonstrated recently [4] that it is definitely quite advantageous to transform the discrete equation into equivalent circuit networks that are subsequently fed into circuit simulators with fast circuit solvers for startlingly short simulation time, compared to traditional finite-element solvers. On the other hand, the construction of this equivalent circuit network could be time consuming and take up considerable space in the circuit simulator [4]. To remedy such pitfalls, we propose in the present work efficient algorithms to transform the coordinates of the discrete equations of the field problem into extremely simple one-dimensional (1-D) circuit networks that can be easily input into circuit simulators.

To solve a field problem using a circuit simulator, we need to have a circuit network equivalent to the discrete finite element model or finite difference model of the field problem. To this end, one method is to develop equivalent circuit networks at the element level; the elemental equivalent circuit networks are then assembled together to form the overall equivalent circuit network for the complete problem [2], [3]. On the other hand, depending on the space dimension of the problem and the basis functions used in the approximation of the trial solution and test function, the elemental equivalent circuit network may be complex [2], leading to a highly complex equivalent circuit network for the whole field problem. If we can transform the coordinates

Manuscript received June 24, 2003. This paper was recommended by Associate Editor Z. Yu.

L. Vu-Quoc is with the Department of Mechanical and Aerospace Engineering, University of Florida, Gainesville, FL 32611 USA (e-mail: vu-quoc@ufl.edu).

Y. Zhai is with the Department of Mechanical and Aerospace Engineering, University of Florida, Gainesville, FL 32611 USA, and also with the Department of Electrical and Computer Engineering, Duke University, Durham, NC <<AU: ZIP CODE??>> USA.

K. D. T. Ngo is with the Department of Electrical and Computer Engineering, University of Florida, Gainesville, FL 32611 USA.

Digital Object Identifier 10.1109/TCAD.2004.828133

of the discrete field equations to obtain the resulting equations in simple form, such as diagonal capacitance matrix and tridiagonal conductance matrix, then the circuit network equivalent to the field problem can be constructed in a much easier fashion.

In this paper, we first review the Falk transformation method [5] in structural dynamics, and establish a formal mathematical framework for this method. Unfortunately, the original Falk method displays a detrimental loss of orthogonality among the generated trial vectors; perhaps for this reason, this method has long fallen into disuse and forgotten. The loss of orthogonality in the original Falk method is similar to that found in the original Lanczos method (e.g., [6] and [7]). Here, we stabilize and generalize the original Falk method by employing a *selective reorthogonalization* procedure to ensure the orthogonality among the generated trial vectors. The generalized Falk method does *not* produce any positive poles, while some other methods do (e.g., [8], [9], etc.). The generalized Falk method enjoys a *faster* transformation time compared to traditional Lanczos-type methods and generates a guaranteed stable and passive 1-D simple circuit system that is equivalent to the original complex system. Even though our coordinate-transformation method is inspired by the Falk method, the derivation of the generalized Falk method is *not* the same as presented in [5] (in German). Our presentation is self-contained and can be read independently from the original paper [5].¹ The generalized Falk method transforms a general finite-element system, represented by possibly full system matrices, into a system with identity capacitance (mass) matrix and tridiagonal conductance (stiffness) matrix while maintaining orthogonality among the trial vectors used for the transformation. In the original Falk method, the transformed capacitance (mass) matrix is a diagonal matrix, but not an identity matrix, i.e., the transformed capacitance (mass) is not uniform. On the other hand, the present generalized Falk method does lead to a uniform transformed capacitance (mass) matrix. For thermal problems, which are governed by system of first-order ODEs in time, the resulting equivalent 1-D circuit network is simple, since it contains only resistors, capacitors, and current sources.² The *stability and passivity* of the resulting 1-D equivalent circuit network is guaranteed since all transformed matrices remain positive definite. Once connected to the circuit part of the overall coupled circuit-field problem, the resulting transformed ordinary differential equations can be efficiently solved using any general-purpose circuit simulator.

Several numerical examples involving both circuit problems and coupled circuit-field problems such as a full bridge converter with IGBT devices and a voltage regulator module (VRM) with MOSFET devices are used to demonstrate the computational efficiency, accuracy, and ease of use of the proposed methodology.

It should be noted that the proposed coordinate-transformation algorithm is especially efficient when used in conjunction with a lumped (e.g., diagonal) capacitance matrix, since it is not costly to invert a diagonal matrix. Several techniques of matrix lumping have been proposed in the literature. Four such

techniques (or matrix diagonalization) were explained in [10, p. 605], with the row-sum technique being a popularly used one. Mass lumping techniques have been extensively developed to increase the efficiency of wave propagation analysis in electromagnetics (e.g., [11], [12]) or in solid and structural mechanics [13], [14]. Mass lumping has also been extensively used in fluid flow and transport problems [15]–[17]. Careful design of mass lumping techniques is important to obtain accurate results, compared to those from the consistent mass [13], [14], [18], [19]. The use of pentadiagonal mass matrix has also been suggested to improve the accuracy, compared to row-sum lumped mass [18]; even in this case, the proposed generalized Falk method still remains effective, since there are efficient algorithms for solving pentadiagonal matrices. Lump mass matrices are also used in multibody dynamics formulation [14].

Krylov-subspace algorithms for modeling and specifically for order reduction have been extensively applied to the context of interconnect modeling in the frequency domain for several years, mostly related to Pade-type approximations and moment-matching methods [8], [20], [21]. Much is known about the properties of the various methods such as the Lanczos and Arnoldi methods. The Lanczos method in particular has been extensively used to compute Pade approximations of linear dynamic circuits. We emphasize here that the proposed method is more advantageous than many Lanczos-type methods, especially for applications to high-frequency coupled circuit-field problems often encountered, e.g., in advanced power electronics circuit design, very large scale integration (VLSI) circuit analysis, etc., since there are no unstable positive poles generated by the generalized Falk method. Many Lanczos-type model-reduction methods, on the other hand, encounter the problem of having positive poles destabilizing the reduced systems [21], and thus require additional special treatment to avoid this problem [22]. Our method does not require any additional treatment, and is more efficient than the Lanczos method. In addition, transient behavior, which is important in power electronics, can be clearly predicted by our method in the time domain.

II. COORDINATE-TRANSFORMATION METHODS

To present our idea, we will use the electrothermal-coupled problem as an example. We will focus on the heat problem to describe the construction of models for the thermal components (e.g., heat sinks) of the overall electrothermal system. These thermal models are obtained from a discretization of the heat-diffusion equation, and can be expressed in several different coordinate systems: the original finite-element coordinate system, and other transformation coordinate systems that will make the subsequent analysis extremely efficient. We first state the heat-diffusion problem, and summarize its finite-element formulation. We then present the generalized Falk method. We derive the connection between the generalized Falk method and the original Falk method. Both methods transform the finite-element coordinate system in such a way to obtain an *identity* capacitance matrix and a *tridiagonal* conductance matrix.

¹For general thermal problems, the capacitance (mass) matrix is invertible.

²For second-order ODEs in time, inductors should be included. The formulation is more complex when the first-order (damping) term is present.

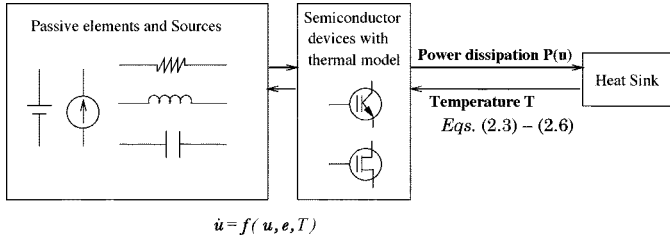


Fig. 1. Coupled electrothermal system.

A. Electrothermal-Coupled Equations

Many electronic circuits contain semiconductor devices (see Fig. 1) can malfunction when heat generated during their operations goes beyond a certain limit. It is, therefore, important to predict, so as to avoid such detrimental self-heating effects. The nonlinear electrothermal coupled system can be generally expressed as

$$\dot{\mathbf{u}} = \mathbf{f}(\mathbf{u}, \mathbf{e}, T) \quad (1)$$

$$\mathbf{P} = \mathbf{P}(\mathbf{u}) \quad (2)$$

where \mathbf{u} is the matrix containing the nodal voltages or currents, \mathbf{e} the electrical input, T the temperature, and \mathbf{P} the electrical power loss. The nonlinear electrical system is governed by the semiconductor equations [partial difference equations (PDEs)] and circuit equations (ODEs). The electrical power loss is originated from the heat generated inside the semiconductor devices. Since the semiconductor pn junction region where most of the heat is generated is small compared to the whole device region, and is close to the top surface of the *Si* chip, the electrical power loss can be assumed to be imported from the top boundary of the *Si* chip, i.e., the electrical power loss is treated as a boundary condition in the thermal problem.

The heat-diffusion problem on a domain Ω with boundary $\partial\Omega = \bar{\Gamma}_1 \cup \bar{\Gamma}_2$ is governed by the PDE

$$\text{div}(\kappa \text{grad } T) = \rho c_p \frac{\partial T}{\partial t} \quad \text{in } \Omega \quad (3)$$

and the boundary conditions

$$\kappa \text{grad } T \bullet \mathbf{n} = \kappa \frac{\partial T}{\partial n} = \frac{P}{A} \quad \text{on } \Gamma_1 \quad (4)$$

$$\kappa \text{grad } T \bullet \mathbf{n} = \kappa \frac{\partial T}{\partial n} = h(T_a - T) \quad \text{on } \Gamma_2 \quad (5)$$

and initial condition

$$T(x, 0) = T_a = 27^\circ\text{C} \quad (6)$$

where $T : \Omega \times \mathbb{R}_+ \rightarrow \mathbb{R}$ is the temperature (a function of space and time), $\kappa : \Omega \rightarrow \mathbb{R}$ the thermal conductance, $\rho : \Omega \rightarrow \mathbb{R}$ the mass density, $c_p : \Omega \rightarrow \mathbb{R}$ the specific heat, $P : \Gamma_1 \times \mathbb{R}_+ \rightarrow \mathbb{R}$ the input power from boundary Γ_1 , A the input-power cross-section area, h the convection coefficient, \mathbf{n} the outward normal vector to the boundary, and T_a the ambient temperature. In the above, the set of real numbers is denoted by \mathbb{R} , with $\mathbb{R}_+ := t \in \mathbb{R} | t \geq 0$, denoting the set of nonnegative numbers. The domain of the heat sink is denoted by $\Omega \subset \mathbb{R}^s$, with $s = 1, 2, 3$ being the space dimension. The boundary $\partial\Omega$ of the heat sink

is decomposed into two parts: Γ_1 for the input power boundary condition (4), and Γ_2 for the convective boundary condition (5).

There are two methods to solve electrothermal-coupled problems: the direct method (fully coupled method) and relaxation method. The direct method is based on the combined modeling of electronic circuits together with the thermal problem in a single simulation tool such as SABER, etc. Here, a single system of algebraic equations encompasses both the electrical components and the thermal components, and is used to simultaneously solve for both the electrical states and the thermal states. In SABER, the electric circuit can be described by a netlist,³ while the thermal problem can be described by an analog behavioral language.⁴ The discretized thermal equations are built into a circuit and system simulator, such as SABER, as supplementary equations. A problem with this method is the thermal modeling process is complicated due to the structure of the *Si* chip, header, and package.

The relaxation method is based on the coupling between a circuit simulator and a field-equation (e.g., thermal) simulator, with each simulator performing the computation independently from each other, and with the results from each simulator passed on to the other simulator to adjust input data before the next computational cycle begins [24], [25]. The circuit part can be simulated with a circuit simulator, while a mechanical sensor or thermal effects can be analyzed by employing the finite element method (FEM) program. Generally, the modeling process for the relaxation method is not so complicated because special simulators have been developed for a particular circuit or field problem. A key point of the relaxation method is how to realize the data transfer, synchronization, and convergence control. The coupling relaxation algorithm requires some repetition of the computed time steps. Furthermore, the data communication between the two simulators will greatly affect the efficiency of the overall computational process. Another disadvantage of the relaxation method is the relatively large simulation time for large-size FE $\ll \text{AU: DEFINE "FE"} \gg$ models.

B. Finite Element Formulation for Thermal System

The semidiscrete equation of the thermal system, derived from a Galerkin finite element projection [2], [26], takes the form

$$\mathbf{C}\dot{\mathbf{d}} + \mathbf{K}\mathbf{d} = \mathbf{f} = \mathbf{I}_p + \mathbf{I}_c \quad (7)$$

$$\mathbf{d}(0) = \mathbf{d}_0 \quad (8)$$

where $\mathbf{C} \in \mathbb{R}^{n \times n}$ is the capacitance matrix, $\mathbf{K} \in \mathbb{R}^{n \times n}$ the conductance matrix, $\mathbf{f} \in \mathbb{R}^{n \times 1}$ the heat supply matrix, \mathbf{I}_p the input power supply from the electrical component, \mathbf{I}_c the heat supply coming from the convective boundary condition, and $\mathbf{d} \in \mathbb{R}^{n \times 1}$ the column matrix of nodal temperatures d_i at the FE node i . Let N_i be the shape function associated with node i , then the temperature field over the domain of the heat problem is approximated by $T(x, t) \cong \sum_{i=1}^n d_i N_i$. The capacitance matrix \mathbf{C} can be realized by capacitor elements, the conductance matrix

³Netlist is a textual description of your design provided as input to the SABER simulator [23].

⁴A behavioral model is one that describes an observed behavior with an appropriate set of equations and coefficients [23].

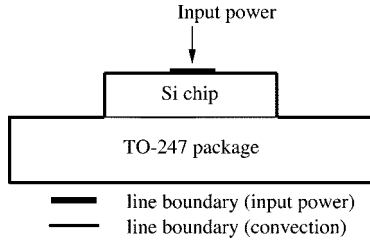


Fig. 2. 2-D thermal-model problem.

\mathbf{K} by resistor elements, and the heat supply vector \mathbf{f} by current sources, so that thermal effects for the semiconductor devices like IGBT and MOSFET can be dynamically incorporated into circuit simulators with thermal connection. The global matrices \mathbf{C} , \mathbf{K} , \mathbf{f} are assembled from the elemental matrices \mathbf{c}_e , \mathbf{k}_e , and \mathbf{f}_e , expressions for the elements of the matrices \mathbf{c}_e , \mathbf{k}_e , and \mathbf{f}_e are given below

$$(\mathbf{c}_e)_{ij} := \rho c_p A \int_{\Omega_e} N_i N_j d\Omega_e \quad (9)$$

$$(\mathbf{k}_e)_{ij} := \kappa A \int_{\Omega_e} \text{grad} N_i \cdot \text{grad} N_j d\Omega_e + h A \int_{\Gamma_2} N_i N_j d\Gamma_2 \quad (10)$$

$$(\mathbf{f}_e)_i := P p_i + \mathbf{h}_i = (\mathbf{I}_p)_i + (\mathbf{I}c)_i \quad (11)$$

where

$$\mathbf{p} = \{p_i\}, \quad (\mathbf{I}_p)_i := P p_i = P \int_{\Gamma_1} N_i d\Gamma_1 \quad (12)$$

$$\mathbf{h} = \{h_i\}, \quad (\mathbf{I}c)_i := h_i = h A T_a \int_{\Gamma_2} N_i d\Gamma_2. \quad (13)$$

Equation (9) and the first term in (10) are the conductive terms. The second terms in (10) and (11) are the convective terms. The first term in (11) is the input power. The thermal network based on the FEM is an equivalent circuit network that yields the same semidiscrete equations (ODEs) resulting from a Galerkin projection using FE basis functions. Similar to FE global matrices, the global thermal network is assembled from elemental networks equivalent to the elemental matrices \mathbf{c}_e , \mathbf{k}_e and \mathbf{f}_e . The coupled electrothermal system is shown in Fig. 1, from which it can be seen that the coupling between these two systems is through the power loss \mathbf{P} and the nodal temperature \mathbf{d} . Recall that the nodal temperatures in \mathbf{d} are system unknowns in a circuit simulator such as SABER, and are solved for simultaneously with the electrical unknowns. As an example of the thermal problem, we consider the *Si* chip and package shown in Fig. 2.

It should be noted that the system capacitance and conductance matrices are symmetric and nonnegative definite, and in general, for any linear first-order ODEs or second-order undamped ODEs, the resulting circuits are RC, LC, or RL networks. It is well known that any passive RC network which is

reduced by congruence transformations (such as our generalized Falk method) remains passive and thus absolutely stable.

Remark 2.1: For a general field problem such as electromagnetics or any linear ODEs, all of the following derivation in this paper should be modified by replacing the system matrices (capacitance and conductance matrices after finite element discretization) by the corresponding FE discretized system matrices. The reader should refer to [27] for the application to the Maxwell equation in electromagnetics model reduction.

In [2], thermal networks equivalent to a discretization of the heat equation by the FEM were presented. The proposed methodology not only solves the field problem, but also provides a natural way to solve the coupled circuit-field problem as a single circuit problem. Depending on the order of interpolation employed, the elemental equivalent circuit networks could be complex, thus making the overall thermal circuit network extremely involved, and not simple to implement in a circuit simulator. If we can transform the original discrete field model into an equivalent simple model (diagonal capacitance matrix and tridiagonal conductance matrix), then the circuit network equivalent to this simple model can be easily constructed.

C. Coordinate Transformation Based on Falk Method

As mentioned in the introduction, when the capacitance (mass) matrix is diagonal, tridiagonal, or even pentadiagonal, and the conductance (stiffness) matrix is full, it is more efficient to transform the system into a diagonal capacitance matrix and a tridiagonal conductance matrix prior to an implementation in a circuit simulator, since the transformed system can be represented by an extremely simple 1-D equivalent circuit network. To this end, we propose a coordinate-transformation algorithm that can be thought of as the generalized Falk method. The proposed coordinate-transformation method transforms any general FE system represented by possibly full capacitance matrix \mathbf{C} and full conductance matrix \mathbf{K} , to a simple system represented by an *identity* capacitance matrix and a *tridiagonal* conductance matrix. The resulting equivalent circuit is a simple 1-D, contains only capacitors, resistors, and current sources. Transient analyzes or eigenvalue problems of such simple 1-D circuit network can be solved extremely fast in circuit simulators.

1) Original Falk Method: The Falk method, first introduced in [5], is mainly the coordinate transformation of any complex mechanical system into an equivalent simple one-dimensional mass-spring system via a class of trial vectors. Due to its simplicity and generality, it has been used for exact model reduction in structural dynamics for mechanical systems [28]. The idea is to generate a transformation matrix in such a way that the transformed system matrices will be diagonal and tridiagonal. Then, another scaling process will be performed to further transform the simplified system matrices such that they can represent a 1-D lumped structure. It can be easily proved that the transformed system has the same eigenvalues as the original system. In [28], the one-dimensional lumped system is further reduced to an arbitrary selected degree of freedom. Unfortunately, the Falk algorithm presented in [28] contains many errors. The readers should refer to [5] for complete derivation of Falk algorithm.

2) *Generalized Falk Method*: Unlike the Lanczos and WYD methods, in which the trial vectors⁵ are generated from the Krylov subspace $\mathcal{K}^{(k)}(K^{-1}C, z_1)$, here, we choose to generate the trial vectors from the Krylov subspace $\mathcal{K}^{(k)}(C^{-1}K, z_1)$: $\mathcal{K}^{(k)}(C^{-1}K, z_1) = \text{span}[z_1, (C^{-1}K)z_1, (C^{-1}K)^2z_1, (C^{-1}K)^3z_1, \dots, (C^{-1}K)^{k-1}z_1]$. We propose the following procedure to generate the trial vector basis.

- 1) Choose a random starting vector or the steady-state solution as starting vector. C -normalize starting vector to obtain z_1 .
- 2) The next vector is generated from the iterative process $Cz_2^* = Kz_1$ to obtain

$$z_2^* = C^{-1}Kz_1. \quad (14)$$

To generate a linearly independent vector basis, the vector z_2^{**} , orthogonal to z_1 , is generated by subtracting from z_2^* the component of z_2^* that is parallel to z_1 (Gram-Schmidt orthogonalization)

$$z_2^{**} = z_2^* - a_1z_1. \quad (15)$$

Set $z_1^T Cz_2^{**} = 0$, to obtain

$$a_1 = \frac{z_1^T Kz_1}{z_1^T Cz_1} = z_1^T Kz_1. \quad (16)$$

Thus,

$$z_2^{**} = C^{-1}Kz_1 - (z_1^T Kz_1) z_1. \quad (17)$$

Finally, normalize z_2^{**} to obtain $z_2 = (z_2^{**})/(\sqrt{z_2^{**T} Cz_2^{**}})$.

- 3) Similar to the generation of z_2^* in (14), subsequent vectors z_i^* , for $i = 3, \dots, n$, are generated by the recurrence relation

$$Cz_i^* = Kz_{i-1} \Rightarrow z_i^* = C^{-1}Kz_{i-1}. \quad (18)$$

We consider two methods to generate vectors z_i that are orthonormal with respect to the matrix C . The first method is similar to the Lanczos method, in which the new vector z_i is obtained by C -orthogonalizing z_i^* generated from (18) with respect to the two previously generated C -orthonormal vectors z_{i-1} and z_{i-2} . First, we generate vector z_i^{**} that is C -orthogonal to the vectors z_i and z_{i-1} . Let

$$z_i^{**} = z_i^* - a_2z_{i-1} - b_2z_{i-2}. \quad (19)$$

With the C -orthogonal conditions

$$\begin{aligned} z_{i-2}^T Cz_i^{**} &= z_{i-2}^T Cz_i^* - a_2z_{i-2}^T Cz_{i-1} - b_2z_{i-2}^T Cz_{i-2} \\ &= 0 \end{aligned} \quad (20)$$

$$z_{i-1}^T Cz_i^{**} = z_{i-1}^T Cz_i^* - a_2z_{i-1}^T Cz_{i-1} - b_2z_{i-1}^T Cz_{i-2}$$

⁵To simplify the description of both the new coordinate-transformation methods, we will use the terminology ‘‘trial vectors’’ to designate the vectors generated by these methods. Thus, Lanczos vectors, WYD vectors, generalized Falk vectors, and original Falk vectors are all trial vectors.

$$= 0 \quad (21)$$

also consider the C -normalization we obtain

$$b_2 = z_{i-2}^T Kz_{i-1} \quad a_2 = z_{i-1}^T Kz_{i-1}. \quad (22)$$

It follows that z_i^{**} can be expressed in terms of the vectors z_{i-1} and z_{i-2}

$$\begin{aligned} z_i^{**} &= C^{-1}Kz_{i-1} - (z_{i-1}^T Kz_{i-1}) z_{i-1} \\ &\quad - (z_{i-2}^T Kz_{i-1}) z_{i-2}. \end{aligned} \quad (23)$$

Next, we C -normalize z_i^{**} to obtain z_i by: $z_i = (z_i^{**})/(\sqrt{z_i^{**T} Cz_i^{**}})$.

In the previous formulation, a trial vector z_i^* is only C -orthogonalized with two trial vectors z_{i-1} and z_{i-2} previously generated. The resulting trial vector is then C -normalized to obtain the next trial vector z_i . Now, instead of C -orthogonalizing with only the previous two trial vectors, we propose a generalization by C -orthogonalizing with all previously generated trial vectors. To this end, we start the generation of the trial vectors in a similar fashion as described above, and let $w_1 = z_1$, and $w_2 = z_2$. From w_3 onward, the generation process begins to differ with the above formulation and we will have $w_i \neq z_i$, for $i = 3, \dots, n$. To generate w_i , first compute $w_i^* = C^{-1}Kw_{i-1}$ as in (18). Next, express w_i^{**} as

$$w_i^{**} = w_i^* - c_{i,i-1}w_{i-1} - c_{i,i-2}w_{i-2} - \dots - c_{i,1}w_1. \quad (24)$$

With the C -orthogonal conditions

$$w_{i-1}^T Cw_i^{**} = w_{i-2}^T Cw_i^{**} = \dots = w_1^T Cw_i^{**} = 0 \quad (25)$$

we can express w_i^{**} in terms of all previously generated vectors w_1, \dots, w_{i-1} as follows:

$$\begin{aligned} w_i^{**} &= C^{-1}Kw_{i-1} - (w_{i-1}^T Kw_{i-1}) w_{i-1} \\ &\quad - (w_{i-2}^T Kw_{i-1}) w_{i-2} - \dots - (w_1^T Kw_{i-1}) w_1. \end{aligned} \quad (26)$$

A C -normalization of w_i^{**} yields w_i as follows:

$$w_i = \frac{w_i^{**}}{\sqrt{w_i^{**T} Cw_i^{**}}}. \quad (27)$$

In the generalized Falk method, the transformed matrix K^* is computed by

$$K^* = W^T KW. \quad (28)$$

We will show that the transformed matrix in the case of the generalized Falk method is tridiagonal and the transformed capacitance matrix $C^* = Z^T CZ = W^T CW = I_n$ is an identity matrix due to the C -orthogonalization process for the generalized Falk method.

Unlike the Lanczos method and the WYD method, in which the generation of the trial vectors can be truncated to obtain a reduced-order model, in the Falk method and the generalized Falk method, a complete set of trial vectors must be generated, and the transformed matrices have the same dimension as in

the original model. The reason is because the Falk and generalized Falk methods generate the trial vectors that are related to the highest eigenpairs first, with the trial vectors related to the lowest eigenpairs appearing toward the end of the generation process. Also, unlike the Lanczos method and WYD method, the transformed matrices in the original Falk method and in the generalized Falk method have the same topology, i.e., a transformed *identity* capacitance matrix and a transformed *tridiagonal* conductance matrix. Since the original Falk method and the generalized Falk method only involve the inverse of the capacitance matrix, it would be especially efficient to generate the transformed matrices if the capacitance matrix were diagonal, tridiagonal, or pentadiagonal. Of course, when a special topology of the conductance matrix \mathbf{C} cannot be taken advantage of in the solution process, \mathbf{C} should be decomposed at the beginning of the generation process, so that only backsubstitutions are carried out within the generation process of the Falk method and the generalized Falk method.

In the generalized Falk method, we orthogonalize the current trial vector with respect to all previously generated vectors. We construct the transformed tridiagonal conductance matrix by formal matrix multiplication.

Remark 2.2: The trial vectors obtained from the original Falk method are different from those obtained from the generalized Falk method because we use a random starting vector in the Falk method and the static solution as starting vector in the generalized Falk method. Even if we used the same starting vector in both methods, the trial vectors are still different from one method to the other, because of the difference in the orthogonalization procedure.

3) *Generalized Falk Method: Conceptual Algorithm:* Similar to the WYD method, the starting vector is the static response obtained from the spatial distribution of the dynamic excitation, and will ensure that the generated trial vectors contain important information of the response.

Algorithm 2.3. Generalized Falk method:
Conceptual Algorithm

- 1 Starting vector $\mathbf{K}\mathbf{w}_1^* = \mathbf{f} \Rightarrow \mathbf{w}_1^* = \mathbf{K}^{-1}\mathbf{f}$.
- 2 \mathbf{C} -normalize \mathbf{w}_1^* to obtain $\mathbf{w}_1 = (\mathbf{w}_1^*)/(\sqrt{\mathbf{w}_1^{*T}\mathbf{C}\mathbf{w}_1^*})$ such that $\mathbf{w}_1^T\mathbf{C}\mathbf{w}_1 = 1$.
- 3 Generate \mathbf{w}_i with $i = 2, \dots, n$ such that $\mathbf{w}_i^* = \mathbf{C}^{-1}\mathbf{K}\mathbf{w}_{i-1}$.
- 4 \mathbf{C} -orthogonalize \mathbf{w}_i^* to obtain $\mathbf{w}_i^{**} = \mathbf{w}_i^* - \sum_{j=1}^{i-1} c_j \mathbf{w}_j$ with $c_j = \mathbf{w}_j^T \mathbf{C} \mathbf{w}_i^*$.
- 5 \mathbf{C} -normalize \mathbf{w}_i^{**} to obtain $\mathbf{w}_i = (\mathbf{w}_i^{**})/(\sqrt{\mathbf{w}_i^{**T}\mathbf{C}\mathbf{w}_i^{**}})$.

4) *Generalized Falk Method: Implementable Algorithm:* The detailed pseudocode for the implementation of the proposed generalized Falk method, with particular attention on computational efficiency, is presented in Algorithm 2.4.

Algorithm 2.4. Generalized Falk method:
Implementable Algorithm

- 1 **Given:** Capacitance \mathbf{C} , conductance \mathbf{K} , and heat supply vector \mathbf{f}
- 2 $\mathbf{K}\mathbf{w}_1 = \mathbf{f} \Rightarrow \mathbf{w}_1 = \mathbf{L}^{-T}\mathbf{L}^{-1}\mathbf{f}$
- 3 \mathbf{C} -normalize $\mathbf{w}_1 = (\mathbf{w}_1)/(\sqrt{\mathbf{w}_1^T\mathbf{C}\mathbf{w}_1})$
- 4 Decompose $\mathbf{C} = \mathbf{L}\mathbf{L}^T$
- 5 Generate the remaining vectors \mathbf{w}_i
- 6 **do** $i = 2, \dots, n$
- 7 Compute $\mathbf{V} = \mathbf{K}\mathbf{w}_{i-1}$
- 8 Compute $\mathbf{w}_i = \mathbf{L}^{-T}\mathbf{L}^{-1}\mathbf{V}$
- 9 \mathbf{C} -normalize \mathbf{w}_i to obtain $\mathbf{w}_i = (\mathbf{w}_i)/(\sqrt{\mathbf{w}_i^T\mathbf{C}\mathbf{w}_i})$
- 10 **do** $j = 1, \dots, i-1$
- 11 Compute $k_{i,j} = \mathbf{w}_j^T \mathbf{C} \mathbf{w}_i$
- 12 Compute $\mathbf{w}_j = \mathbf{w}_j - k_{i,j} \mathbf{w}_i$
- 13 **end**
- 14 **end**

D. Relationship Between Falk Method and Generalized Falk Method

Here, we show that the generalized Falk method leads to transformation matrices having the same topology (diagonal capacitance and tridiagonal conductance) as those in the original Falk method. Even though the topology of the transformed matrices in both methods are the same, the numerical values of the coefficient in these matrices are *not* the same, since the generated trial vectors are not the same. Furthermore, the generalized Falk method leads to an *identity* capacitance matrix, instead of just a *diagonal* capacitance matrix obtained by the original Falk method. In other words, the generalized Falk method leads to a uniform distribution of capacitance (equal to one), whereas the original Falk method does *not*. The orthogonalization step in the generalized Falk method as presented above can be written in matrix form as follows:

$$\mathbf{C}^{-1}\mathbf{K}[\mathbf{w}_1|\mathbf{w}_2|\dots|\mathbf{w}_r] = [\mathbf{w}_1|\mathbf{w}_2|\dots|\mathbf{w}_r]\mathbf{H} \quad (29)$$

with

$$\mathbf{H} = \begin{bmatrix} c_{1,1} & c_{2,1} & c_{3,1} & \cdot & c_{r,1} \\ c_{1,2} & c_{2,2} & c_{3,2} & \cdot & c_{r,2} \\ 0 & c_{2,3} & c_{3,3} & \cdot & \cdot \\ 0 & 0 & c_{3,4} & \cdot & \cdot \\ \cdot & \cdot & \cdot & \cdot & \cdot \\ 0 & 0 & \cdot & c_{r-1,r} & c_{r,r} \end{bmatrix}_{r \times r} \quad (30)$$

or simply

$$\mathbf{C}^{-1}\mathbf{K}\mathbf{W} = \mathbf{W}\mathbf{H} \quad (31)$$

where \mathbf{H} in (30) is a matrix in upper Hessenberg form, which is an upper triangular matrix with nonzero entries on the subdiagonal. Premultiplying (31) by $\mathbf{W}^T\mathbf{C}$, we obtain

$$\mathbf{W}^T\mathbf{C}\mathbf{C}^{-1}\mathbf{K}\mathbf{W} = \mathbf{W}^T\mathbf{C}\mathbf{W}\mathbf{H}. \quad (32)$$

The left-hand side of (32) must be symmetric since \mathbf{K} is symmetric. Using the fact that $\mathbf{W}^T\mathbf{C}\mathbf{W} = \mathbf{I}$, we obtain

$$\mathbf{W}^T\mathbf{K}\mathbf{W} = \mathbf{H} \quad (33)$$

which must be symmetric. The only way that the upper Hessenberg matrix \mathbf{H} is symmetric is that \mathbf{H} is tridiagonal; i.e.,

$$\mathbf{H} = \mathbf{T}_n. \quad (34)$$

It follows from (34) that the generalized Falk method is equivalent to the original Falk method.

For the heat equation given by (7), the transformed thermal system expressed in original Falk coordinates and in generalized Falk coordinates are obtained by premultiplying (7) with \mathbf{W}^T , and by using the substitution $\mathbf{d} = \mathbf{W}\mathbf{y}$. Consider the fact $\mathbf{C}^* = \mathbf{W}^T \mathbf{C} \mathbf{W} = \mathbf{I}$, we obtain

$$\boxed{\mathbf{I}\dot{\mathbf{y}} + \mathbf{K}^* \mathbf{y} = \mathbf{W}^T \mathbf{f}} \quad (35)$$

where $\mathbf{K}^* = \mathbf{W}^T \mathbf{K} \mathbf{W} = \mathbf{T}_n$. For both the original Falk method and the generalized Falk method, the transformed capacitance matrix \mathbf{C}^* is an identity matrix, and the transformed conductance matrix \mathbf{K}^* is tridiagonal. The two transformed matrices \mathbf{K}^* are different from each other though, since the generated generalized Falk vectors are not the same as the generated original Falk vectors.

Remark 2.3: It should be noted that the coordinate-transformed Arnoldi algorithm in [8] and the block-Arnoldi-based passive reduced-order interconnect macromodeling algorithm (PRIMA) in [29] only preserves half as many as matched number of moments by the block Lanczos algorithm. Therefore, accuracy in the Pade approximation through moment matching is not preserved. The generalized Falk method generates a reduced-order model directly through the WYD process with a full orthogonalization and a selective reorthogonalization [30]. Time-domain transient analysis is performed with the reduced-order model without solving any eigenvalue problems or system transfer functions.

III. STABILITY AND REORTHOGONALIZATION

A. Lanczos Method and WYD Method

It is well known that both the Lanczos method and the WYD method will exhibit a loss of \mathcal{C} -orthogonality among the generated vectors after a finite number of steps. The Lanczos vectors, which are orthogonal in exact arithmetic, not only lose their orthogonality as their generation progresses, but may even become linearly dependent. It is not surprising that the same is true for the WYD method, since the two methods are related to each other. The generated vectors, once becoming linearly dependent, are no longer useful since they cannot be used in a coordinate transformation of a FE system [6], [26], [30]–[32].

For both the Lanczos method and the WYD method, selective reorthogonalization is necessary to maintain orthogonality among the generated (trial) vectors. For the WYD method, while a static-solution starting vector can produce a set of trial vectors (i.e., WYD vectors) that capture much of the dynamical features of the system, a randomly generated starting vector usually produces a set of trial vectors with a better orthogonality property in the sense that these trial vectors remain orthogonal to each others longer, before a loss of orthogonality begins to set in.

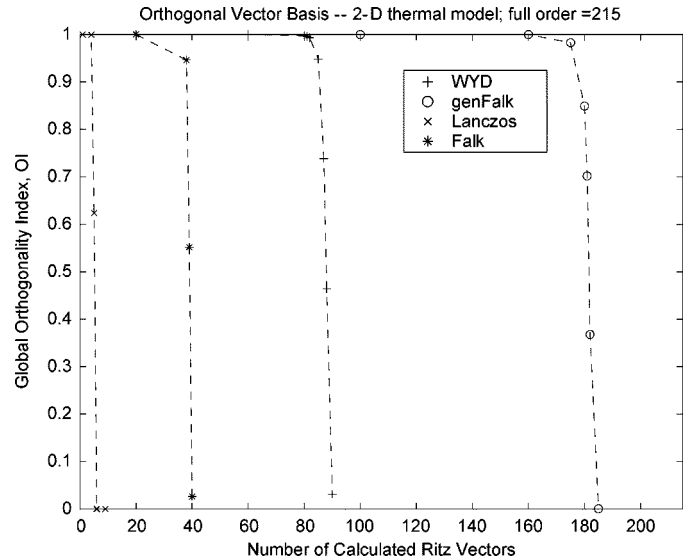


Fig. 3. Loss of orthogonality in WYD/Lanczos and Falk/generalized Falk methods without reorthogonalization.

In general, a loss of orthogonality occurs when the spectral content of a starting vector has been exhausted. Thus, with a randomly generated starting vector for use in the WYD method, instead of a static-solution, it is possible to obtain the complete set of WYD vectors, even without *reorthogonalization*. The reason is because a randomly-generated vector tend to have nonzero components along *all* eigendirections. We note that without reorthogonalization or selective reorthogonalization, the Lanczos method always suffers from a loss of orthogonality, even with randomly-generated starting vector. The reason for this remarkable stability of the WYD method is that each generated WYD vector is orthogonalized with all previously generated WYD vectors, whereas a generated Lanczos vector is orthogonalized to only the last two previously generated vectors.

If the static solution is used as the starting vector, a loss of orthogonality generally occurs when about half of the WYD vectors have been generated without reorthogonalization (see Fig. 3). Even with reorthogonalization, the linear independence of the generated WYD vector as monitored by a global Orthogonality Index (OI)—defined as the ratio of the lowest eigenvalue of $\mathbf{C}^* = \mathbf{W}^T \mathbf{C} \mathbf{W}$ over its largest eigenvalue⁶—is sensitive to the orthogonalization tolerance (see Fig. 4). To generate a set of linearly independent WYD vectors, we need to be careful in choosing the orthogonalization tolerance. This tolerance should not be too large (in which case we do not have a good set of linearly independent WYD vectors), nor too small (in which case the computational cost would be too high).

B. Original Falk Method and Generalized Falk Method

Without reorthogonalization, loss of orthogonality among the generated trial vectors also occur in the original Falk and generalized Falk methods, but much later as compared to the traditional Lanczos and WYD methods. In [6], it is shown that the loss of orthogonality in the Lanczos process is also a measure of the convergence of the Ritz values (i.e., approximated

⁶In principle, \mathbf{C}^* is identity matrix. Because of loss of orthogonality, \mathbf{C}^* in practice can not be exactly identity.

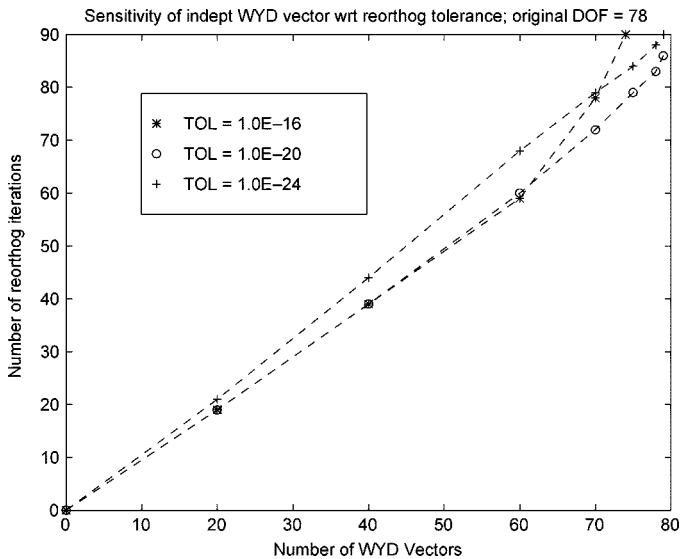


Fig. 4. Sensitivity of independent WYD vectors with respect to reorthogonal tolerance.

eigenvalues). The original Falk and generalized Falk processes tend to converge to the highest eigenvalues, with slower rate of convergence compared to the traditional Lanczos and WYD methods, which converge to the lowest eigenvalues. To demonstrate the different behavior in the loss of orthogonality, we consider a 2-D thermal finite-element model employed in [2]. Shown in Fig. 7 is the FE mesh with 368 triangular elements and 215 nodes.⁷ The resulting OI for the original Falk or generalized Falk method, and for the traditional Lanczos/WYD methods is plotted in Fig. 3, where an earlier loss of orthogonality in the Lanczos method and original Falk method can be observed. Static starting vectors are used for WYD and generalized Falk methods. Random starting vectors are used for Lanczos and original Falk methods.

For the Lanczos method, instead of full reorthogonalization, a more cost-effective selective reorthogonalization has been proposed ([6], [31], [33], [34]) by monitoring the components of each generated Lanczos vector along the previously generated Lanczos vectors. A reorthogonalization of the just generated Lanczos vector is only effected against those previously generated Lanczos vectors for which these components are larger than certain tolerance.

Remark 3.1: It is shown in [30] that working directly with \mathbf{T}_r is less stable than working with \mathbf{K}^* matrix, especially if the eigenspectrum has close eigenvalues. It is well known that, theoretically, the Lanczos method cannot treat multiple eigenvalues; however, in practice, the multiple eigenvalues are determined by round-off errors. In [35], a modified version of the WYD method is used in which the method starts with block initial vectors, in a similar format to the subspace iteration method, but carries on iterations one by one. This way, multiple eigenpairs may be extracted. The convergence of the modified WYD method was better than the Lanczos method, and was an order of magnitude faster than the standard subspace iteration method.

⁷Each node has one unknown voltage.

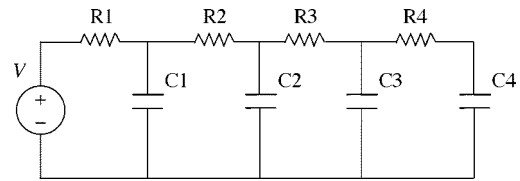


Fig. 5. Simple circuit shows that PVL algorithm can produce unstable positive poles even if original systems are passive.

TABLE I
GENERATED POLES FROM VARIOUS KRYLOV-BASED MODEL REDUCTION
METHODS: PVL METHOD, ARNOLDI PROCESS AND
GENERALIZED FALK METHOD

Krylov methods	Negative poles				Positive poles
	1	2	3	4	1
exact	-2.6055	-1.8198	-0.9928	-0.4856	--
PVL	--	-2.0028	--	-0.4856	2.0360
Arnoldi	--	-1.9779	-0.9978	-0.4856	--
GenFalk	-2.6187	-1.8390	--	-0.4864	--

Block Lanczos can solve multiple eigenpairs, however like subspace iteration, the modified WYD method converges faster than the Block Lanczos method.

C. Pade Via Lanczos (PVL) and Arnoldi Algorithms

It is well known that the Lanczos-type algorithms based on direct Pade approximation does not guarantee passivity of the reduced-order model and hence its stability. Unstable positive poles could be generated in the AWE and PVL method. Post-processing is needed to eliminate the unstable poles. The coordinate-transformed Arnoldi algorithm ([8]) generates guaranteed stable reduced-order models of *RLC* circuits, but it cannot guarantee passivity [29]. The Arnoldi-type PRIMA in [29] includes guaranteed passivity but eigendecomposition of the reduced-order model is needed for system transfer function in the Laplace domain. The generalized Falk algorithm introduced here generates guaranteed passive and thus stable transformed model. Transient analysis in the time domain is performed easily and accurately in a circuit simulator without solving any expensive eigenvalue problem. Fig. 5 shows two simple circuit examples to demonstrate the advantage of the generalized Falk method over the PVL method.

Table I shows clearly that unlike the PVL algorithm, the generalized Falk algorithm does not introduce positive poles that destabilize the originally stable system. In [8], the RC circuit in Fig. 5 showed that the PVL algorithm can produce an unstable model even if the system is described by a symmetric positive definite matrix, while our generalized Falk algorithm does not suffer from positive poles.

IV. NUMERICAL EXAMPLES WITH COORDINATE TRANSFORMATION

In this section, we present numerical examples to illustrate the efficiency of the coordinate-transformation methods in electrothermal simulations of power electronic circuits and systems. thermal models, coupled with the other circuit network, the circuit temperature distribution as the currents and

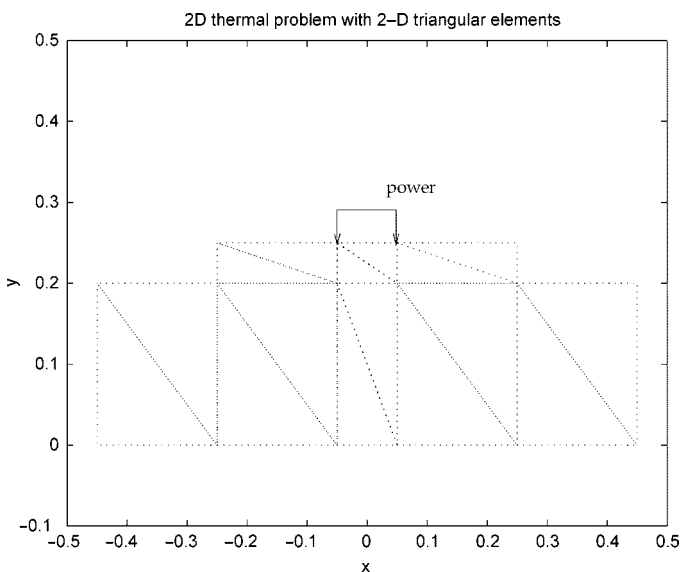


Fig. 6. Coarse FE mesh for 2-D thermal problem.

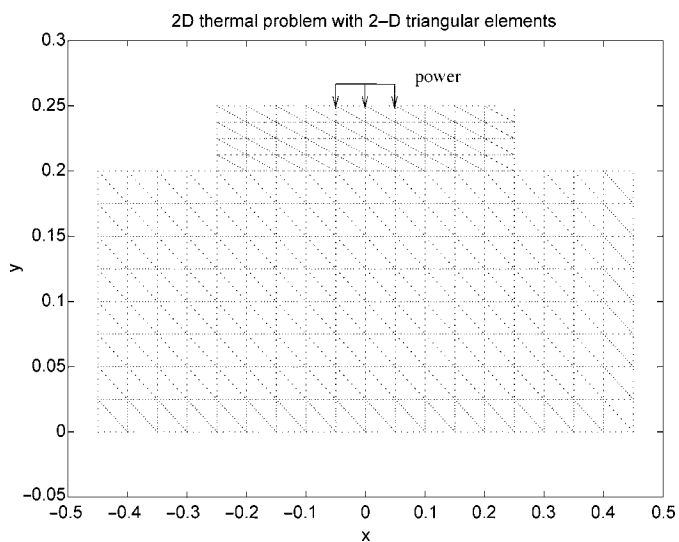


Fig. 7. FE mesh2 for 2-D thermal problem.

Simulation times Simulation times for both full-order models and the transformed models are presented for comparison.

A. Verification of Thermal Component Models

To verify the thermal-component model, obtained from the algorithms described in previous sections, we consider the *Si* chip and TO247 package shown in Fig. 2 (2-D problem). Figs. 6 and 7 show the finite element meshes of this device: Mesh1 (Fig. 6) contains 16 linear triangular elements and 16 nodes;⁸ Mesh2 (Fig. 7) contains 368 linear triangular elements and 215 nodes. Two types of model are used in the analysis: The full-order model and the transformed model (1-D equivalent circuit with the same number of dofs) obtained from using the generalized Falk/original Falk method. The input power at the top of the *Si* chip is $P = 10$ W, distributed uniformly over an area $A = 0.1$ cm². All types of model were implemented in SABER

⁸Since each node has one unknown voltage, the number of nodes is also the number of equations.

TABLE II
MATLAB CPU TIMES USED TO GENERATE THE TRANSFORMED
MODELS WITH REORTHOGONALIZATION

simulation models	Generalized Falk	Falk	WYD	Lanczos
Coord. transf.	613.33s	609.71s	1,854.1s	1,834.4s

and MATLAB (See [2] for the implementation of the full-order model in SABER). The nodal temperatures at the top of the *Si* chip from two types of model agree well with each other.

Table II gives the transformation time for a thermal component model with 1226 dofs from various Krylov transformation methods: WYD method, Lanczos method, generalized Falk method and original Falk method with selective reorthogonalization. The tolerance for reorthogonalization is 10^{-16} and the number of reorthogonalization is 5. It clearly shows that the original/generalized Falk methods are more advantageous compare to the WYD/Lanczos methods. This is mainly because that unlike the WYD/Lanczos methods, in the original/generalized Falk methods, we do not need to invert the system conductance matrix \mathbf{K} .

B. Electrothermal Simulation of a Full-Bridge Converter

To meet the continuing demand of further reduction in size and weight and of increased efficiency in power electronic devices, switched-mode technology for regulated power supply has received considerable attention due to the possibility of achieving lossless power conversion. The switched-mode regulator employs duty cycle control of a switching element to block the flow of energy and thus achieve regulation. It has the added advantage when applied to offline applications of giving significant size reduction in the voltage transformer and energy storage elements [36].

Among power-electronic switching devices, IGBT is highly suited to high-power and high-voltage applications. A full-bridge transformer-isolated buck converter with four IGBT devices, shown in Fig. 8, is simulated with the circuit simulator SABER [3]. Fig. 9 shows the driving voltages for the full-bridge converter, with the on time $T_{\text{on}} = 15$ μs , the dead time-period $\Delta = 10$ μs when all switches are off, and the switching time $T_s = 50$ μs . During the first subinterval $0 < t < T_{\text{on}}$, transistors IGBT1 and IGBT4 conduct, and the transformer primary voltage is V_{in} . The voltage appearing across each half of the center-tapped secondary winding is nV_{in} , with n the primary to secondary turn ratio and the polarity mark at positive potential. Diode D_5 is, therefore, forward biased, and D_6 is reverse biased. The voltage across the filter is then equal to nV_{in} , and the output filter inductor current $i(t)$ flows through diode D_5 . For the second subinterval $T_{\text{on}} < t < T_{\text{on}} + \Delta$, all four transistors are switched off and, hence, the transformer voltage is $V_T = 0$. During $T_{\text{on}} + \Delta < t < T_s - \Delta$, transistors IGBT2 and IGBT3 and diode D_6 conduct, thus, the transformer primary voltage is $-V_{in}$.

The parameters used are input voltage $V_{\text{in}} = 100$ V dc, primary to secondary turn ratio $n_1/n_2 = 2$, gate resistances $R_{\text{gi}} = 100$ Ω , low-pass filter inductance $L_o = 300$ μH , low-pass filter capacitance $C_o = 100$ μF , and output resistance $R_o = 5$ Ω . These values are chosen so that thermal

run-away⁹ occurs. Thermal run-away cannot be predicted from a conventional circuit simulation with a fixed temperature. The electrothermal IGBT model in SABER is used in the simulation with the following parameters [23]: [*tauhl*: the high-level excess carrier lifetime; *tauhlexp*: temperature exponent for *tauhl*; *wb*: metallurgical base width; *nb*: base-doping concentration; *a*: device-active area; *agd*: gate-drain-overlap active area; *isne*: emitter electron saturation current; *isnetexp*: temperature exponent for *isne*; *vt*: MOSFET channel-threshold voltage; *vtco*: temperature coeff. for *vt*; *rs*: intrinsic anode series resistance; *theta*: empirical parameter which models transconductance reduction due to the transverse electric field in the MOSFET; *thetac*: temp. exponent for *theta*; *kf*: empirical factor to model ratio of *kp* in triode region to that in saturation for MOSFET ($= kp, \text{linear}/kpt$); *kftexp*: temperature exponent for *kf*; *kp*: MOSFET channel transconductance in saturation region; *kptexp*: temperature exponent for *kp*; *cgs*: gate to source capacitance; *cox*: gate drain oxide capacitance; *vtd*: gate drain overlap depletion threshold; *vtdco*: temp. coeff. for *vtd*; *bvf*: *bvftexp*: *bvn*: avalanche multiplication exponent; *bvntexp*: temp. exponent for *bvn*; *tnom*: temperature for which parameters apply; *alpha*: temp. exponent for mobilities; *gmin*: minimum slope for MOSFET current]; *tauhl* = 7.1 μ , *tauhlexp* = 1.5, *wb* = 10 m, *nb* = 2.0e14, *a* = 0.1, *agd* = 0.05, *isne* = 10 f, *isnetexp* = 0.5, *vt* = 5.0, *vtco* = -0.009, *rs* = 0.01, *theta* = 0.01, *thetac* = 0, *kf* = 2.0, *kftexp* = 0, *kp* = 0.25, *kptexp* = 1.5, *cgs* = 1 n, *cox* = 2 n, *vtd* = 0, *vtdco* = 0, *bvf* = 1.0, *bvftexp* = 0.35, *bvn* = 4.0, *bvntexp* = 0, *tnom* = 27, *alpha* = 2.54, and *gmin* = 1 p.

The short-circuit-test simulation result of the IGBT model with the above parameters is similar to that in [1]. By using the generalized-Falk transformed model, we also established the efficiency in electrothermal coupled simulations. Table III gives the comparison between the transient-simulation times for the original full 2-D equivalent circuit thermal model and for the generalized-Falk¹⁰ transformed model of the heat sinks in the four IGBT devices of the full-bridge converter. It is important to note that in Table III, the SABER simulation time does *not* include the transformation time from physical coordinates to trial-vector (generalized-Falk or Lanczos) coordinates, but does include the transformation time from trial-vector coordinates back to physical coordinates. The SABER simulation time for the Lanczos method is approximately the same for the generalized Falk method, but the transformation time for the Lanczos method is longer than that for generalized Falk method, as shown in Section IV-A (see Table II).

C. Electrothermal Simulation of a VRM

In order to meet faster and more efficient data-processing demands, modern microprocessors are being designed with lower voltage and higher current implementations. Meanwhile, more

⁹Thermal run-away is a major cause of fires and failure of electronic equipment. It occurs when the equipment continues to generate heat faster than it can be dissipated. The temperature will continue to rise until the equipment fails or a fire breaks out.

¹⁰The original Falk method yields the same results as the generalized Falk method.

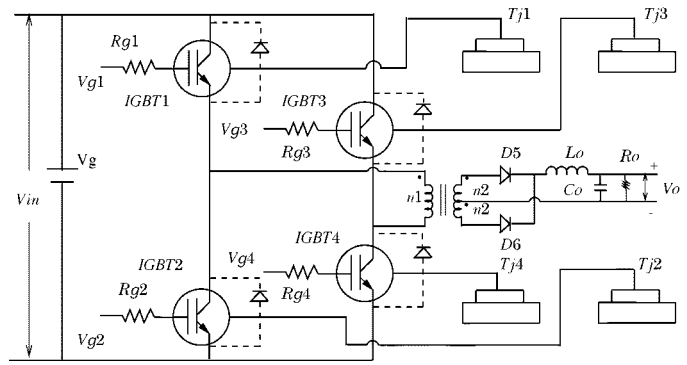


Fig. 8. Full-bridge converter with four IGBTs as switching devices.

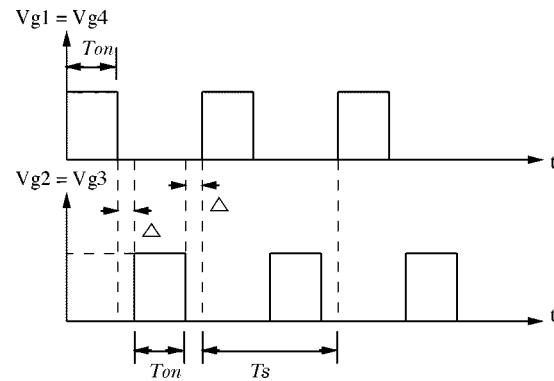


Fig. 9. Waveforms of the driving voltages for the full-bridge converter.

TABLE III
FULL-BRIDGE CONVERTER: COMPARISON OF SIMULATION TIMES (WITHOUT TRANSFORMATION TIMES) BETWEEN FULL MODEL AND TRANSFORMED MODEL: MESH1 WITH 16 NODES AND MESH2 WITH 215 NODES

simulation models	SABER transient analysis	
	mesh1	mesh2
full model	291s	1190s
generalized Falk	116s	327s
Lanczos	131s	337s

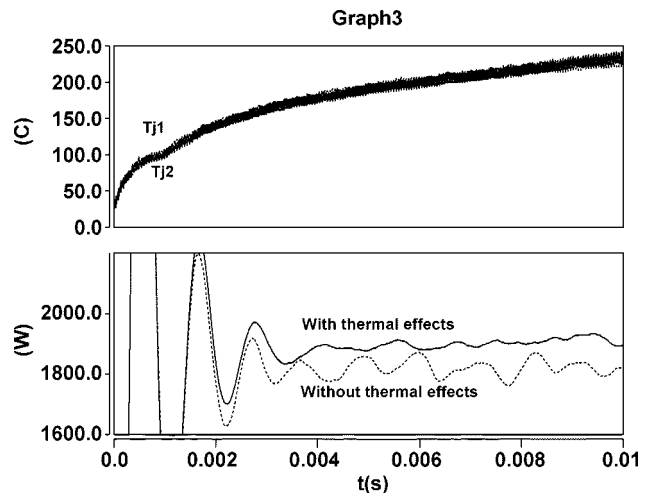


Fig. 10. Full bridge converter: simulation results from SABER.

devices are packed on a single processor chip and the processors operate at higher operating frequencies. To minimize the effects of the interconnection parasitics, also to achieve a highly

accurate supply voltage regulation that cannot be accomplished by a centralized power system, special on-board power supply modules, VRMs, located on the motherboard next to the load, is required to provide lower voltages with higher current capability for microprocessors [37]. In a distributed power system, the dc-dc converter produces an intermediate voltage, which appears at the computer backplane. Each card contains high-density dc-dc converters that produce locally regulated low voltages. Generally, since the board real estate is relatively expensive, the on-board converter modules (the VRM) is required to have high-power density and to operate with high efficiency. To meet these requirements and to provide fast transient response, the power conversion must be performed at high-switching frequency, thus presenting a serious design challenge. The reason to keep the regulated voltage fixed is because each silicon device has a maximum and a minimum voltage limit, and each silicon device is most efficient at a certain fixed-voltage range. If the output voltage goes out of the device-voltage tolerance, the device will blow up.

The VRM shown in Fig. 11 <<AU: FIG 10 MUST BE CITED BEFORE FIG 11!>> [38] was simulated in SABER, using our equivalent-circuit model for the thermal component. The waveforms of the driving voltages are shown in Fig. 12. The operating frequency for the simulated VRM is 500 kHz. The following major components of the VRM power stage were selected: Switch SW-2XIRF7811, Synchronous rectifier SR-4XIRF7811, inductor $L = 500$ nH, output filter capacitor $C = 100$ μ F, input voltage $V_g = 60$ V, and load resistance $R = 15$ Ω .

Table IV gives the comparison between the transient simulation times of the full 2-D thermal model and of that by generalized Falk transformed model of the VRM.

D. Comparison of Results From Circuit Simulator

In this section, we compare the results of the above-described examples obtained from full-order models and from the proposed coordinate-transformed models, with two types of models implemented in the circuit simulator SABER.

Fig. 10 shows the S_i -junction temperature of heat sink T_{j1} and T_{j2} versus simulation time and the converter output power ($V_o * I_o$) versus simulation time for the full bridge converter, both with thermal effects and without thermal effects. It clearly shows the output power difference which will be neglected in the simulation without considering the electrothermal coupling of the power switching devices. Also, big ripples exist from the simulation without thermal effects, which are undesired.

Fig. 13 shows a more significant increase of the MOSFET bulk-drain total energy dissipation against simulation time for both the full-order model and the generalized Falk-transformed model obtained from FE Mesh2 for the buck-converter VRM example.

Fig. 14 shows the converter regulated voltage output with and without thermal effects and S_i -junction temperature rise versus simulation time. It slightly shows the decrease of the output voltage with time, which means the loss of energy due to heat dissipation.

These figures clearly show that thermal coupling is essential for an accurate simulation of a power electronic system. With

TABLE IV
BUCK-CONVERTER VRM: COMPARISON OF SIMULATION TIMES (WITHOUT TRANSFORMATION TIMES) BETWEEN FULL MODEL AND TRANSFORMED MODEL: MESH1 WITH 16 NODES AND MESH2 WITH 215 NODES

simulation models	SABER transient analysis	
	mesh1	mesh2
full model	1280s	6690s
generalized Falk	258s	1130s
Lanczos	259s	1160s

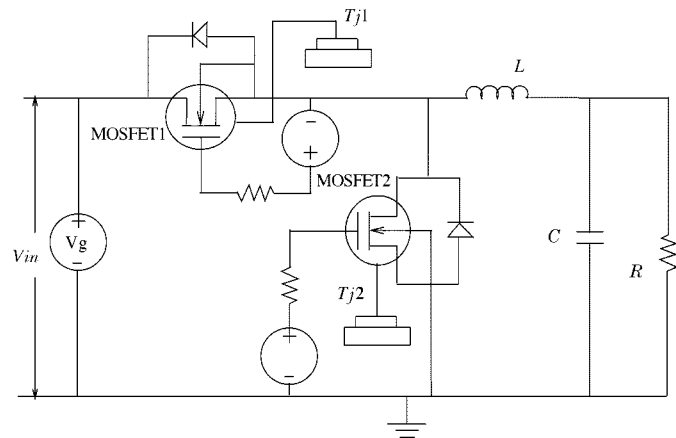


Fig. 11. Buck-converter VRM with synchronous rectifier.

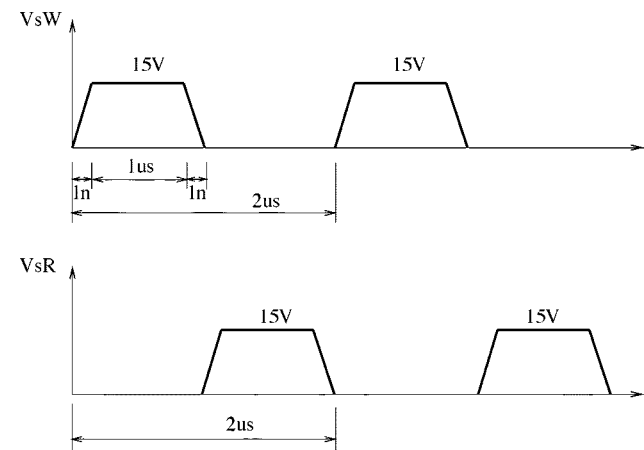


Fig. 12. Waveforms of the driving voltages for the Buck-converter VRM.

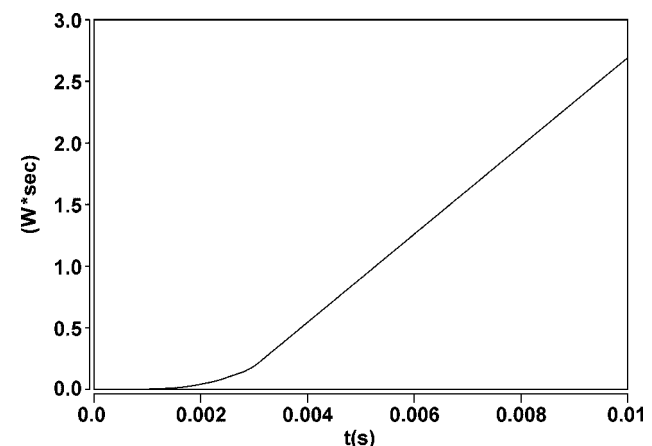


Fig. 13. VRM: MOSFET bulk-drain total energy dissipation versus simulation time by transformed model obtained from FE mesh2 with generalized Falk transformation.

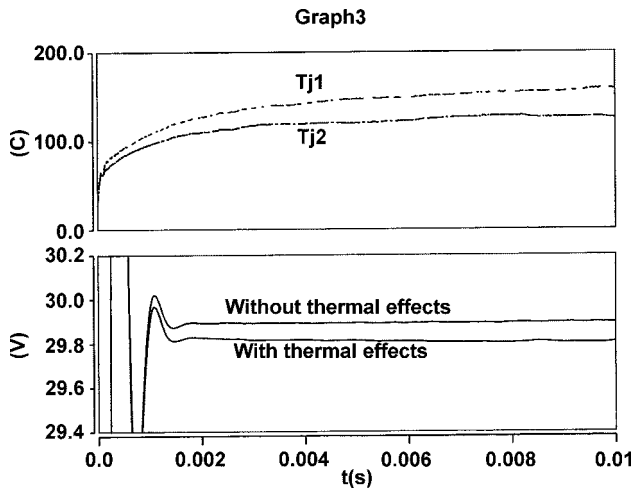


Fig. 14. VRM: Output voltage and S_i -junction temperature versus simulation time by transformed model obtained from FE mesh2 with generalized Falk transformation.

our proposed generalized Falk transformation, the speed-up ratio for the simulation of the full bridge converter is 2.5 for FE mesh1 and 3.64 for FE mesh2. The speed-up ratio for the simulation of the VRM is about 5 for FE mesh1 and 6 for FE mesh2.

It is noted that our circuit examples involve highly nonlinear component (IGBT and VRM), and the speed up ratio is based on the reduction in the total simulation time, but not based on just the reduction of the field (heat sink) part. On the other hand, the time reduction demonstrated in VLSI computer-aided design literature with the Lanczos-type algorithms based on moment-matching technique was restricted to the linear part of the circuit (interconnect) only.

V. CLOSURE

We proposed a generalized Falk method to transform any complex system of linear first-order ODEs or second-order undamped ODEs, resulting from the discretization of field PDEs, represented by possibly full-system matrices—capacitance and conductance matrices in heat problems, or mass and stiffness matrices in structural dynamics and electromagnetics—into a simple 1-D equivalent circuit system with the capacitance (mass) matrix being identity and conductance (stiffness) matrix being tridiagonal.

The generalized Falk method computes accurately higher-order poles or eigenvalues of the original full system matrices. It is well known that truncating the higher-order poles using certain model-reduction methods can lead to unstable reduced-order models. Unlike other Lanczos-type methods, the generalized Falk method does not produce any unstable positive poles, and is more efficient than the Lanczos method. The generalized Falk method, therefore, generates guaranteed stable and passive reduced-order models.

It is easy to construct the equivalent circuit network for the resulting 1-D system, which is then combined with the circuit part of the overall coupled circuit-field problem. The resulting combined circuit can be solved easily and efficiently by any circuit simulator. The proposed generalized Falk method makes

it easy to incorporate coupled circuit-field problems into circuit simulator, whether the order of the model for the field problem is reduced or not.

Without reorthogonalization, the loss of orthogonality in the generalized Falk method is much less severe than in the original Falk method and in the WYD/Lanczos methods. As a result, the necessity for reorthogonalization of the trial vectors is more important in the original Falk method and in the WYD/Lanczos methods, as compared to the generalized Falk method. Of course, the generalized Falk method with reorthogonalization would be even better.

Several numerical examples involving both circuit problems and coupled circuit-field problems are described in details to illustrate the mentioned advantages of the proposed generalized Falk method.

ACKNOWLEDGMENT

The authors thank the research support of the National Science Foundation.

REFERENCES

- [1] A. Hefner and D. Blackburn, "Simulating the dynamic electrothermal behavior of power electronic circuits and systems," *IEEE Trans. Power Electron.*, vol. 8, pp. 376–385, <<AU: MONTH?>> 1993.
- [2] J. T. Hsu and L. Vu-Quoc, "A rational formulation of thermal circuit models for electrothermal simulation—Part I: Finite element method," *IEEE Trans. Circuits Syst. I*, vol. 43, pp. 721–732, Sept. 1996.
- [3] —, "A rational formulation of thermal circuit models for electrothermal simulation—Part II: Model reduction techniques," *IEEE Trans. Circuits Syst. I*, vol. 43, pp. 733–744, Sept. 1996.
- [4] A. Ekinci and A. Atalar, "An electrical circuit theoretical method for time- and frequency-domain solutions of the structural mechanics problems," *Int. J. Numer. Methods Eng.*, vol. 45, pp. 1485–1507, 1999.
- [5] V. S. Falk, "Die Abbildung eines allgemeinen Schwingungssystems auf eine einfache Schwingerkette" (in German), *Ingenieur-Archiv*, vol. 23, pp. 314–328, 1955.
- [6] C. C. Paige, "Computational variants of the Lanczos method for the eigenproblem," *Numer. Algorithm*, vol. 10, pp. 373–381, 1972.
- [7] H. D. Simon, "The Lanczos algorithm with partial reorthogonalization," *Math. Computat.*, vol. 42, no. 165, pp. 115–142, 1984.
- [8] L. Silveira, M. Kamon, I. Elfadel, and J. White, "A coordinate-transformed Arnoldi algorithm for generating guaranteed stable reduced-order models of RLC circuits," *Comput. Methods Appl. Mech. Eng.*, vol. 169, pp. 377–389, 1999.
- [9] R. W. Freund, "Reduced-order modeling techniques based on Krylov subspaces and their use in circuit simulation," *Appl. Computat. Control, Signals, Circuits*, vol. 1, pp. 435–498, 1999.
- [10] O. C. Zienkiewicz and R. L. Taylor, *The Finite Element Method*, 4th ed. New York: McGraw-Hill, 1989.
- [11] A. Bossavit and L. Kettunen, "Yee-like schemes on a tetrahedral mesh, with diagonal lumping," *Int. J. Numer. Modeling: Electron. Networks, Devices Fields*, vol. 12, no. 1, pp. 129–142, 1999.
- [12] A. Nicolas, L. Nicolas, and C. Vollaire, "Explicit 2-D finite element time domain scheme for electromagnetic wave propagation," *IEEE Trans. Magn.*, vol. 35, pp. 1538–1541, May 1999.
- [13] S. W. Key, M. W. Heinstein, C. M. Stone, F. J. Mello, M. L. Blanford, and K. G. Budge, "Suitable low-order, tetrahedral finite element for solids," *Int. J. Num. Methods Eng.*, vol. 44, no. 12, pp. 1785–1805, 1999.
- [14] E. J. Haug and W. Pan, "Optimal inertia lumping from modal mass matrices for structural dynamics," *Comput. Methods Appl. Mech. Eng.*, vol. 163, no. 1–4, pp. 171–191, September 1998.
- [15] D. W. Pepper and D. B. Carrington, "Application of h-adaptation for environmental fluid flow and species transport," *Int. J. Numer. Methods Fluids*, vol. 31, no. 1, pp. 275–283, 1999.
- [16] M. C. Boufadel, M. T. Suidan, and A. D. Venosa, "Numerical model for density-and-viscosity-dependent flows in two-dimensional variably saturated porous media," *J. Contaminant Hydrol.*, vol. 37, no. 1, pp. 1–20, 1999.

- [17] V. Lagendijk, D. Jansen, C. Forkel, and J. Koengeter, "New multi-continuum model for the simulation of unsaturated flow in fractured permeable systems," presented at the Proc. 2nd Int. Water Resources Eng. Conf., Memphis, TN, Aug. 3–7, 1998.
- [18] M. A. Christon, "Influence of the mass matrix on the dispersive nature of the semi-discrete, second-order wave equation," *Comput. Methods Appl. Mech. Eng.*, vol. 173, no. 1, pp. 147–166, 1999.
- [19] M. J. S. Chin-Joe-Kong, W. A. Mulder, and M. van Veldhuizen, "Higher-order triangular and tetrahedral finite elements with mass lumping for solving the wave equation," *J. Eng. Math.*, vol. 35, no. 4, pp. 405–426, 1999.
- [20] L. T. Pillage and R. A. Rohrer, "Asymptotic waveform evaluation for timing analysis," *IEEE Trans. Computer-Aided Design*, vol. 9, pp. 352–366, Apr. 1990.
- [21] P. Feldmann and R. Freund, "Reduced order modeling of large linear subcircuits via a block Lanczos algorithm," in *Proc. IEEE Design Automation Conf.*, 1995, pp. 474–479.
- [22] Z. Bai, P. Feldmann, and R. Freund, "Stable and passive reduced-order models based on partial Padé approximation via the Lanczos process," Bell Labs., Lucent Technol., Murray Hill, NJ, Tech. Rep. 97/3-10, 1997.
- [23] *SABER Users Manual*, Analogy Inc., Beaverton, OR, 1997.
- [24] S. Wünsche, C. Clauss, P. Schwarz, and F. Winkler, "Electro-thermal circuit simulation using simulator coupling," *IEEE Trans. VLSI Syst.*, vol. 5, pp. 277–282, Sept. 1997.
- [25] —, "Microsystem design using simulator coupling," in *Proc. IEEE Eur. Design Test Conf.*, vol. 17, 1997, pp. 113–118.
- [26] T. J. R. Hughes, *The Finite Element Method*. Englewood Cliffs, NJ: Prentice-Hall, 1987.
- [27] Y. Zhai and L. Vu-Quoc, "Finite element formulation and model-order reduction for coupled nonlinear electromagnetic problems with static hysteresis," *Int. J. Numer. Methods Eng.*, 2003.
- [28] S. L. Chen and M. Geradin, "An exact model reduction procedure for mechanical systems," *Comput. Methods Appl. Mech. Eng.*, vol. 143, pp. 69–78, 1997.
- [29] A. Odabasioglu, M. Celik, and L. T. Pileggi, "Prima: Passive reduced-order interconnect macromodeling algorithm," *IEEE Trans. Computer-Aided Design*, vol. 17, pp. 645–653, Aug. 1998.
- [30] P. Leger, "The use of load dependent vectors for dynamic and earthquake analyses," Ph.D. dissertation, <<AU: DEPT?>> Univ. of California, Berkeley, Nov. 1986.
- [31] C. C. Paige, "Error analysis of the Lanczos algorithm for tridiagonalizing a symmetric matrix," *Numer. Algorithm*, vol. 18, pp. 341–349, 1976.
- [32] B. N. Parlett, *The Symmetric Eigenvalue Problem*. Englewood Cliffs, NJ: Prentice-Hall, 1980.
- [33] C. C. Paige, "Accuracy and effectiveness of the Lanczos algorithm for symmetric eigenproblems," *Linear Alg. Its Applicat.*, vol. 34, pp. 235–258, 1980.
- [34] B. Parlett and D. Scott, "The Lanczos algorithm with selective orthogonalization," *Math. Computat.*, vol. 33, no. 145, pp. 217–238, 1979.
- [35] J. Xu, "An improved method for partial eigensolution of large structures," *Comput. Structures*, vol. 32, no. 5, pp. 1055–1060, 1989.
- [36] R. W. Erickson and D. Maksimovic, *Fundamentals of Power Electronics*, 2nd ed. Norwell, MA: Kluwer, 2001.
- [37] X. Zhou, P. Wong, X. Peng, F. Lee, and A. Huang, "Investigation of candidate vrm topologies for future microprocessors," *IEEE Trans. Power Electron.*, vol. 11, pp. 328–337, <<AU: MONTH?>> 2000.
- [38] Y. Panov and M. M. Jovanovic, "Design considerations for 12-V/1.5-V, 50-A voltage regulator modules," in *Proc. 15th Annu. IEEE Appl. Power Electron. Conf. Expo.*, vol. 1, 2000, pp. 39–46.



Loc Vu-Quoc received the Diplome d'Ingenieur in structural engineering (with highest honors) from the Institut National des Science Appliquees, Lyon, France, in 1979, the M.S. degree in structural mechanics from the Illinois Institute of Technology, Chicago, <<AU: YEAR?>>, and the M.S. degree in electrical engineering and computer science and the Ph.D. degree in structural engineering and structural mechanics from the University of California, Berkeley, in 1985 and 1986, respectively.

He was with the Centre Technique des Industries Mecaniques, Senlis, France where he developed finite element codes from 1979 to 1981. After two years of postdoctoral work at Stanford University and the University of California, Berkeley, he joined the University of Florida, Gainesville, in 1988, and is currently Professor of Mechanical and Aerospace Engineering. His current research interests are in applied/computational electromagnetics/mechanics and in power-electronics simulation.

Prof. Vu-Quoc received the NSF Presidential Young Investigator Award in 1990.



Yuhu Zhai received the B.E. and M. E. degrees in engineering mechanics from Huazhong University of Science and Technology, <<AU: LOCATION?>> in 1990 and 1993, respectively, and the M.S. and Ph.D. degrees in engineering mechanics from the University of Florida, Gainesville, in 2001 and 2003, respectively.

Before joining the Computational Laboratory for Electromagnetics and Solid Mechanics, University of Florida, he was a Civil Engineer, working on the design and structural analysis of thermal power plants at North China Electric Power Design Institute for five years. He is currently a Postdoctoral Research Associate with the Department of Electrical and Computer Engineering, Duke University, Durham, NC. His research interests include computational electromagnetics and solid mechanics, remote sensing, multi-physics domain simulation, and multiscale methods in fracture mechanics.



Khai D. T. Ngo (S'82–M'84–SM'02) received the B.S. degree from California State Polytechnic University, Pomona, in 1979, and the M.S. and Ph.D. degrees from the California Institute of Technology, Pasadena, in 1980 and 1984, respectively, all in electrical and electronics engineering.

He was a Member of the Technical Staff, General Electric Corporate Research and Development Center, Schenectady, NY, from 1984 to 1988. Since 1988, he has been with the University of Florida, Gainesville, where he is currently a Professor of Electrical and Computer Engineering. His current research interests are magnetic materials and components, energy reclamation, power converters, and power integrated circuits.